metals

MDPI

Article

The Influence of Segregation Bands and Hot Rolling on the Precipitation of Secondary Phases during Aging at 750 °C for Nickel Alloy 625

Simon Malej [1,*], Jožef Medved [2], Barbara Šetina Batič [1], Franc Tehovnik [1], Franci Vode [1], Jaka Burja [1] and Matjaž Godec [1]

1 Institute of Metals and Technology, Lepi pot 11, 1000 Ljubljana, Slovenia; barbara.setina@imt.si (B.Š.B.); franc.tehovnik@imt.si (F.T.); franci.vode@imt.si (F.V.); jaka.burja@imt.si (J.B.); matjaz.godec@imt.si (M.G.)
2 Faculty for Natural Sciences and Technology, Aškerčeva cesta 11, 1000 Ljubljana, Slovenia; jozef.medved@ntf.uni-lj.si
* Correspondence: simon.malej@imt.si; Tel.: +386-14-701-995

Received: 11 January 2019; Accepted: 7 March 2019; Published: 11 March 2019

Abstract: For Inconel 625, where the γ'' and δ phases precipitate, the influence of prior hot rolling on the process is not well covered. The influence of segregation bands and prior hot rolling on the precipitation of secondary phases during aging at 750 °C for different times was investigated. Prior hot-rolling was conducted on a hot rolling mill at 1050 °C and 1150 °C with three different deformation levels. The hot rolled samples were aged at 750 °C for 1, 5, 25 and 125 h. The γ'' precipitated in both the deformed and recrystallized grains in the segregation bands containing a high concentration of niobium and molybdenum and a lower concentration of nickel, chromium and iron. The opposite was observed between the segregation bands where no γ'' precipitate was found. There was a smooth transition in the density and the size of the γ'' particles in the deformed grains at the border of the segregation bands, while a more complex transition occurred in the recrystallized grains. This occurred in the area where the average niobium concentration decreased from 4.5 to 2.7 wt. %, which influenced the mechanical properties.

Keywords: nickel-based superalloy; hot rolling; recrystallization; segregation; precipitation

1. Introduction

The precipitation and growth of different phases in superalloys is influenced by both the chemical composition and the deformation [1–4]. The influence of prior deformation on the precipitation of secondary phases is not a well-researched problem. Precipitation can impact on the mechanical properties, corrosion resistance and microstructural stability of a component during service.

The Inconel 625 alloy was originally designed as a solid-solution-strengthened, nickel-based superalloy with good mechanical properties, corrosion and oxidation resistance [5]. However, Inconel 625 is prone to a complex precipitation processes due to a high niobium content in combination with aluminum, titanium and carbon. Intermetallic phases like $Ni_2(Cr,Mo)$ with a Pt_2Mo structure, γ'' (Ni_3Nb) with a DO_{22} structure and δ (Ni_3Nb) with a $D0_a$ structure, as well as secondary carbides like $M_{23}C_6$ and M_6C, precipitate at different temperatures [6–11]. Primary MC carbides, M(C,N) carbo nitrides, TiN nitrides and the Laves phase form during casting [12,13]. The heterogeneous precipitation of γ'' occurs during aging in the temperature range between 700 and 750 °C [1,10]. In the early stages of aging, the γ'' phase preferentially precipitates on dislocations, sub-grain boundaries and twin boundaries. The critical nucleus size is an important factor in the precipitation process. The volume, interfacial and volume strain free energy influences the critical nucleus size. Structures like dislocations and grain boundaries can reduce the critical nucleus size and enable enhanced precipitation, while providing a large number of nucleation sites [2,14–16].

Nickel-based superalloys have complex microstructure evolution processes during hot working [17]. Due to a low stacking-fault energy, dynamic recrystallization is the dominant softening mechanism during hot deformation [18]. At the start of the hot deformation, work hardening (WH) and recovery compete with one another. During the WH stage, the dislocation density increases through the activation of different slip systems [19]. Due to the lack of softening by recovery, the forces quickly rise to a critical value, where the dynamic recrystallization initiates [20–22]. Two mechanisms of dynamic recrystallization are known for Inconel 625: discontinuous dynamic recrystallization and continuous dynamic recrystallization. The discontinuous recrystallization involves the formation of new nuclei via grain-boundary bulging, while the continuous recrystallization takes place via the generation of low-angle grain boundaries that eventually transform into high-angle grain boundaries.

Two deformation temperatures and three different levels of deformation were used in this research in order to capture the microstructure before and after the initiation of the dynamic recrystallization. The ageing temperature of 750 °C was chosen because the heterogeneous precipitation of γ'' takes place. The influence of the prior hot deformation and segregation bands on the precipitation of secondary phases was studied, and the effect of secondary phases on the tensile strength was analyzed.

2. Materials and Methods

Inconel 625 in the mill-annealed state was used in this research. The chemical composition is given in Table 1. Hot rolling was conducted on a 95 kW laboratory rolling mill (Schmitz, Berlin, Germany). The diameter of the rolls was 296 mm and the rotating speed was 27 min^{-1}. Plates with dimensions of 150 × 53 × 20.7 mm^3 were heated in a preheated resistance furnace and held at the hot-rolling temperatures of 1050 and 1150 °C for 30 min. After 30 min of annealing, three plates were hot rolled with three different levels of deformation. The Table 2 summarizes the level of deformation and the strain rate achieved during hot rolling. Samples for aging (55 × 12 mm^2) were cut from the plate with an abrasive water jet. Aging was carried out in a preheated resistance furnace at 750 °C for 1, 5, 25 and 125 h. After hot rolling and aging, the specimens were cooled in water.

Table 1. Chemical composition of the nickel-based superalloy 625 used in this study and the limiting composition of Inconel 625 in wt. %.

Alloy	Cr	Mo	Fe	Nb	Ti	Al	Si	Mn	C	Ni
Used alloy	21.5	8.2	5.0	3.4	0.14	0.09	0.08	0.05	0.009	Bal.
Inconel 625	20.0–23.0	8.0–10.0	5.0 max.	3.15–4.15	0.4 max.	0.4 max.	0.5 max.	0.5 max.	0.1 max	Bal.

Table 2. Temperature of hot rolling and level of deformation and average strain rate achieved during hot rolling.

Temperature of Hot Rolling	1050 °C	1050 °C	1050 °C	1150 °C	1150 °C	1150 °C
Level of deformation (%)	4.6	12.7	23.5	5.7	14.4	25.2
Strain rate (s^{-1})	1.63	2.7	3.66	1.81	2.87	3.8

Samples were prepared for tensile tests and microscopy. The tensile tests were conducted on an INSTRON 8802 testing machine (Instron, Norwood, MA, USA). The samples for the scanning electron microscopy (SEM) observations were etched with a solution of 15 ml HCl, 10 ml $C_3H_6O_3$, 5 ml HNO_3 and 1–2 ml $C_3H_8O_3$. Final polishing with a colloidal silica suspension (OP-S) solution was applied for the preparation of the samples for electron-backscatter diffraction (EBSD) mapping. The microstructure investigation was carried out on a JEOL JSM 6500F field-emission scanning electron microscope (JEOL, Tokyo, Japan) with an HKL Nordlys II EBSD camera (Oxford Instruments, High Wycombe, UK), Chanel 5 software (Oxford Instruments, High Wycombe, UK) and an Oxford Instruments energy-dispersive spectroscopy (EDS) system with Inca software (Inca Energy 450, Oxford Instruments, High Wycombe, UK). During the EBSD mapping the samples were tilted by 70° and an accelerating voltage of 15 kV with a probe current of 1.5 nA was used. In order to observe the dislocations, the Electron Channeling Contrast Imaging (ECCI) was carried out on a Carl Zeiss Cross Beam 550 scanning electron microscope (Zeiss, Oberkochen, Germany). The samples for ECCI were prepared with final polishing using OP-S (the duration of polishing was 20 min). The ECCI was conducted with a working distance of 6 mm, an accelerating voltage of 30 kV and a probe current of 3.5 nA. MTEX software (mtex-5.1.1., free Matlab toolbox) was used for the data processing resulting from the EBSD mapping [23]. Grain orientation spread (GOS) was implemented for the separation of the recrystallized grains from the deformed grains. GOS is the average difference in the orientation between different points in the grain. Deformed grains have a higher GOS compared to the recrystallized grains [24,25]. High-angle grain boundaries (HAGBs) were characterized as boundaries having a misorientation of more than 15°. A deviation of 3° was used for the coincidence site lattice for the Σ3 (CSL3) determination [26,27]. The size of the γ'' precipitates was measured along the longer axis of the ellipsoid particle. All together, 60 particles were measured, and the average size and the standard deviation were calculated.

3. Results and Discussion

3.1. Microstructure Evolution during Hot Rolling

The microstructure evolution of the plates hot rolled at 1050 and 1150 °C with three different deformation levels is shown in orientation image microscopy (OIM) maps with inverse pole figure (IPF-Z) coloring (Figure 1a–g). A 0.65° GOS difference was used to separate the recrystallized grains from the deformed grains (Figure 2a,b). The plate hot rolled at 1050 °C and with a 4.6% deformation did not contain recrystallized grains (Figure 1a). Before dynamic recrystallization, the GOS shows only one peak, but as soon as the recrystallization occurs, a bimodal distribution is visible in the GOS (Figure 2a,b).

The ECCI image (Figure 3a,b) shows the difference between the deformed grains and the recrystallized grains. The deformed grains have a higher orientation changes which influences the electron diffraction and the signal on the backscatter electron image (Figure 3a). When the background is dark enough (i.e., when the Bragg condition is met), the dislocations (Figure 3b) and other crystal defects can be seen [28,29]. The scattering of the electrons is different due to the distortion of the crystal lattice caused by the dislocation strain field. Figure 3a,b shows a higher density of dislocations in the deformed grains compared to the recrystallized grains.

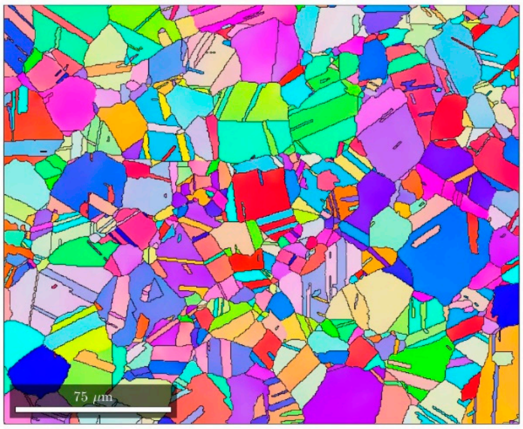

(**a**)

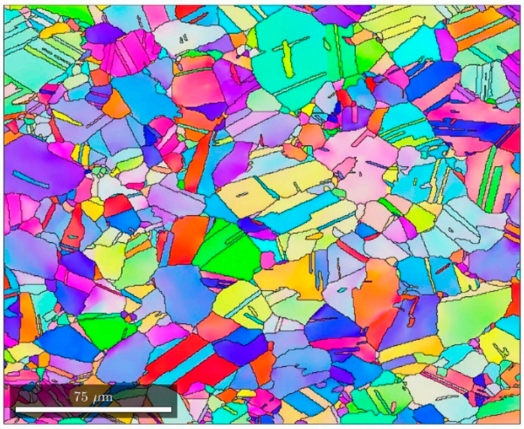

(**b**)

Figure 1. *Cont.*

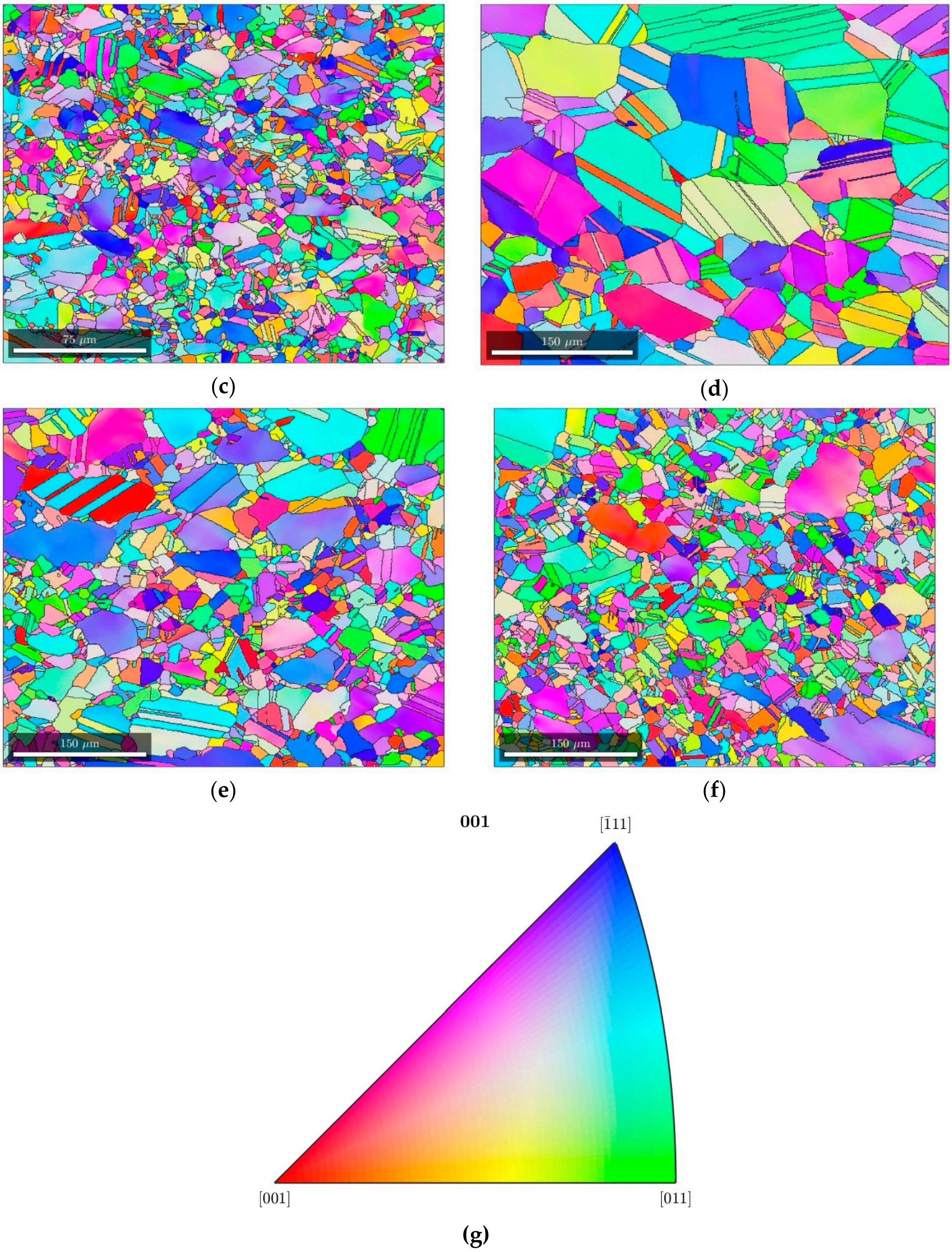

Figure 1. OIM maps with IPF-Z coloring of plates hot rolled at 1050 °C and with a deformation levels of 4.6 (**a**), 12.7 (**b**) and 23.5% (**c**) and hot rolled at 1150 °C with a deformation levels of 5.7 (**d**), 14.4 (**e**) and 25.2% (**f**) and IPF-Z color triangle (**g**).

The occurrence of twins (CSL3 boundaries) is an important phenomenon during hot deformation. The increasing deformation level decreases the fraction of CSL 3 at both 1050 and 1150 °C (Figure 4a,b). However, the highest HAGB fraction was reached at a deformation level of 12.7% for the plate hot rolled at 1050 °C. For the plated hot rolled at 1050 °C, the highest fraction of HAGB was achieved with a deformation level of 14.4%. When the deformed and recrystallized grains are separated the fraction of twins and HAGBs stay roughly the same for the recrystallized grains. Meanwhile, the deformed grains contain an even higher fraction of HAGBs [30].

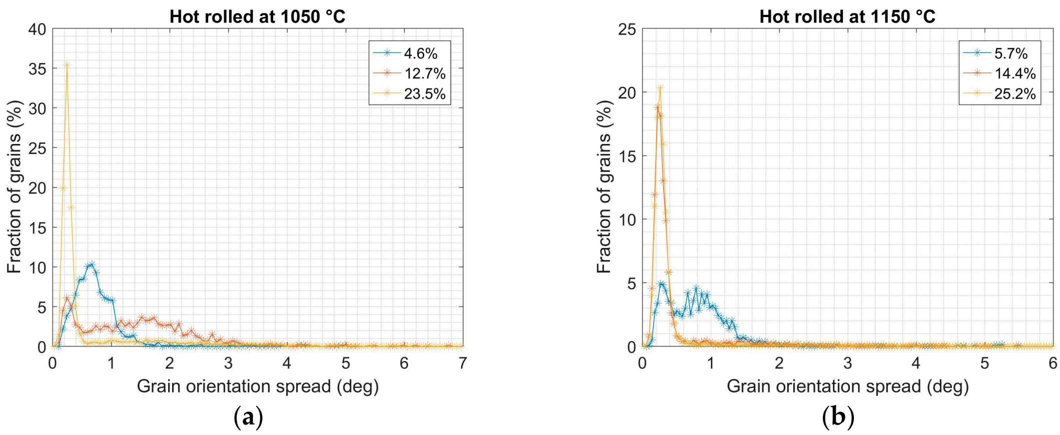

Figure 2. GOS for plates hot rolled at 1050 °C with deformation levels of 4.6%, 12.7% and 23.5% (**a**) and hot rolled at 1150 °C with deformation levels of 5.7%, 14.4% and 25.2% (**b**).

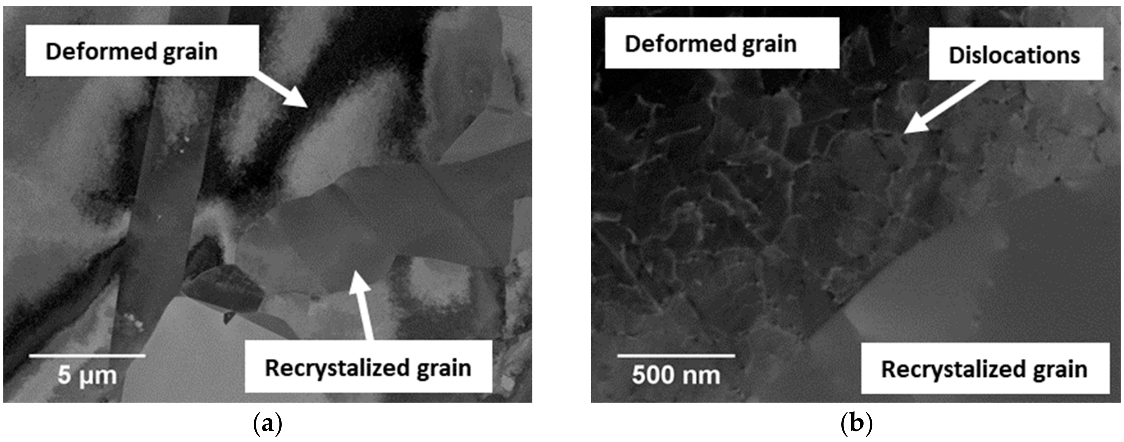

Figure 3. ECCI image of plate hot rolled at 1050 °C with a deformation level of 23.5% showing deformed grains and recrystallized grains (**a**). A large number of dislocations in the deformed grain (**b**).

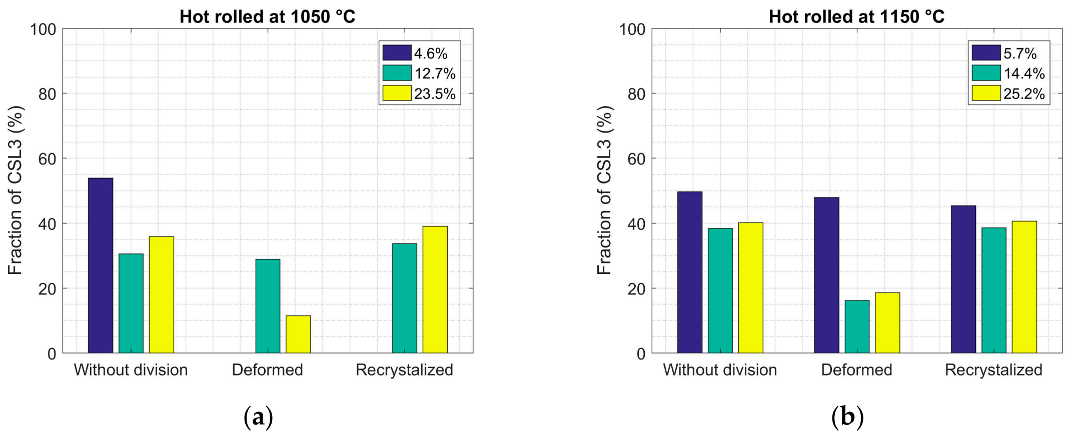

Figure 4. Fraction of CSL3 boundaries without division, in deformed and recrystallized grains for plates hot rolled at 1050 °C (**a**) and 1150 °C (**b**) with different deformation level.

3.2. The Precipitation of Secondary Phases during Aging at 750 °C

Bright bands with very high number of fine γ'' phase precipitates appear after aging at 750 °C for 1 h (Figure 5a–c). In contrast, the areas between the segregation bands contain very little or no γ'' phase precipitates (Figure 5a). The segregation bands contain a higher concentration of Nb and Mo, thus enhancing the precipitation of γ'' [5]. Nb and Mo segregations occur during solidification [31–33]. During hot rolling, these areas are deformed, forming long bands. Some segregation bands contain primary M(C,N) carbo nitrides (Figure 6a,b, Table 3), MC carbides (Figure 7a,c, Table 3), Laves phase (Figure 7a,b, Table 3), and some TiN nitrides [13]. The main difference between the carbides like MC carbide and the Laves phase is the crystal structure. The Laves phase has a hexagonal crystal structure (P64/mmc), compared to the cubic structure of the primary MC carbide (Fm3m) and the γ-matrix (Figure 7d–f). During high-temperature annealing before hot rolling, the primary MC carbides, M(C,N) carbo nitrides and the Laves phase partially dissolute and contribute to even higher concentrations of Nb in the segregation bands (Figures 5b and 6a).

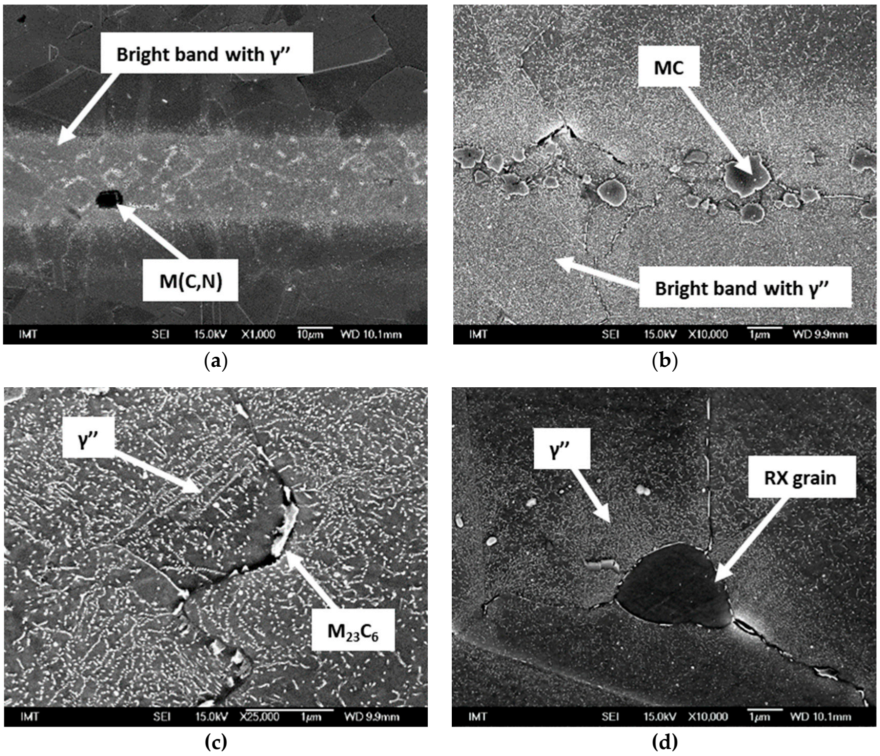

Figure 5. The precipitation of γ'' in the segregation band for the samples hot rolled at 1050 °C with the deformation level of 4.6% and aged at 750 °C for 1 h (**a**). Primary MC carbides in the samples hot rolled at 1150 °C with the deformation level of 5.7% and aged at 750 °C for 1 h (**b**). Bulged grain boundary in the samples hot rolled at 1150 °C with the deformation level of 5.7% and aged at 750 °C for 1 h (**c**). Recrystallized grain with no γ'' precipitates in the sample hot rolled at 1050 °C with the deformation level of 12.7% and aged at 750 °C for 1 h (**d**).

Table 3. Composition of different phases obtained by EDS analysis (wt. %).

Phases	Ni	Cr	Mo	Fe	Nb	Ti	Si
M(C,N) (Figure 6a)	Bal.	2.0	0.0	0.0	38.7	55.6	-
MC (Figure 7a)	Bal.	2.8	3.0	0.6	83.1	4.5	-
Laves (Figure 7a)	Bal.	11.8	26.8	1.5	33.2	-	0.6
$M_{23}C_6$ (Figure 8d)	Bal.	33.8	12.0	3.9	3.8	-	-
δ (Figure 13e)	Bal.	16.0	9.6	2.8	9.5	-	-

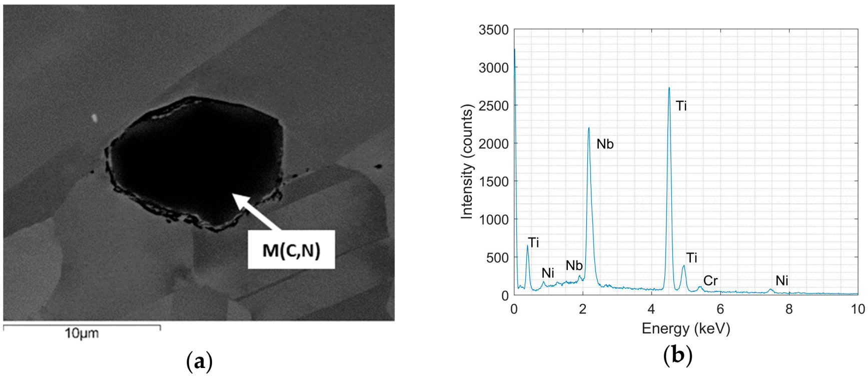

Figure 6. Backscatter-electron image (BEI) of a M(C,N) carbo nitride particle in plate hot rolled at 1050 °C with the deformation level of 4.6% (not aged) (**a**) and EDS spectrum of a M(C,N) carbo nitride (**b**).

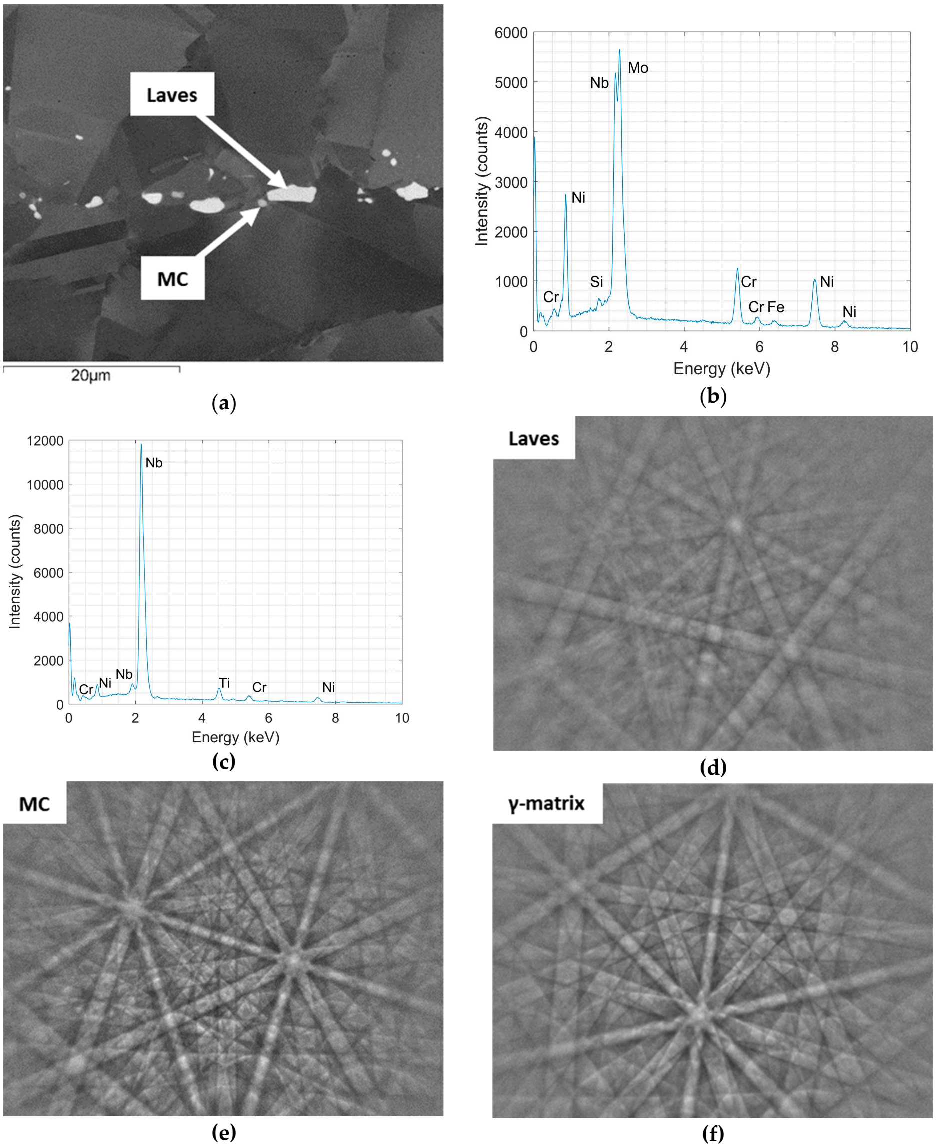

Figure 7. BEI image of the Laves phase and the primary MC carbides in the segregation band of plate hot rolled at 1050 °C with the deformation level of 4.6% (not aged) (**a**). The EDS spectrum for the Laves particle (**b**) and the primary MC carbide (**c**) in Figure 7a. The Kikuchi pattern of the Laves particle (**d**), the primary MC carbide (**e**) and the γ matrix (**f**) in Figure 7a.

At the edge of the segregation bands, the recrystallized grains are clearly visible after aging for 1+ h at 750 °C (Figures 5d and 8a,c). The deformed grains have a high density of dislocations and contain large numbers of fine γ'' precipitates (Figures 5a–d and 8b,c). The γ'' precipitates form along twins and dislocations (Figure 8a) [1,10]. This is why the recrystallized grains contain only a few or no precipitates (Figures 5d and 8a). After 1+ h of aging at 750 °C, the secondary $M_{23}C_6$ carbides and the δ phase start to precipitate on the grain boundaries (Figures 5c and 8a). With longer aging times (5+ h) the secondary $M_{23}C_6$ carbides become coarser (Figure 8b,c). The secondary $M_{23}C_6$ carbides contain high contents of Cr and Mo (Figure 8d, Table 3). In the samples hot rolled at 1150 °C with the deformation level of 5.7% and aged at 750 °C for 1+ h, the secondary $M_{23}C_6$ carbides started to form a continuous line at the grain boundaries (Figure 8b).

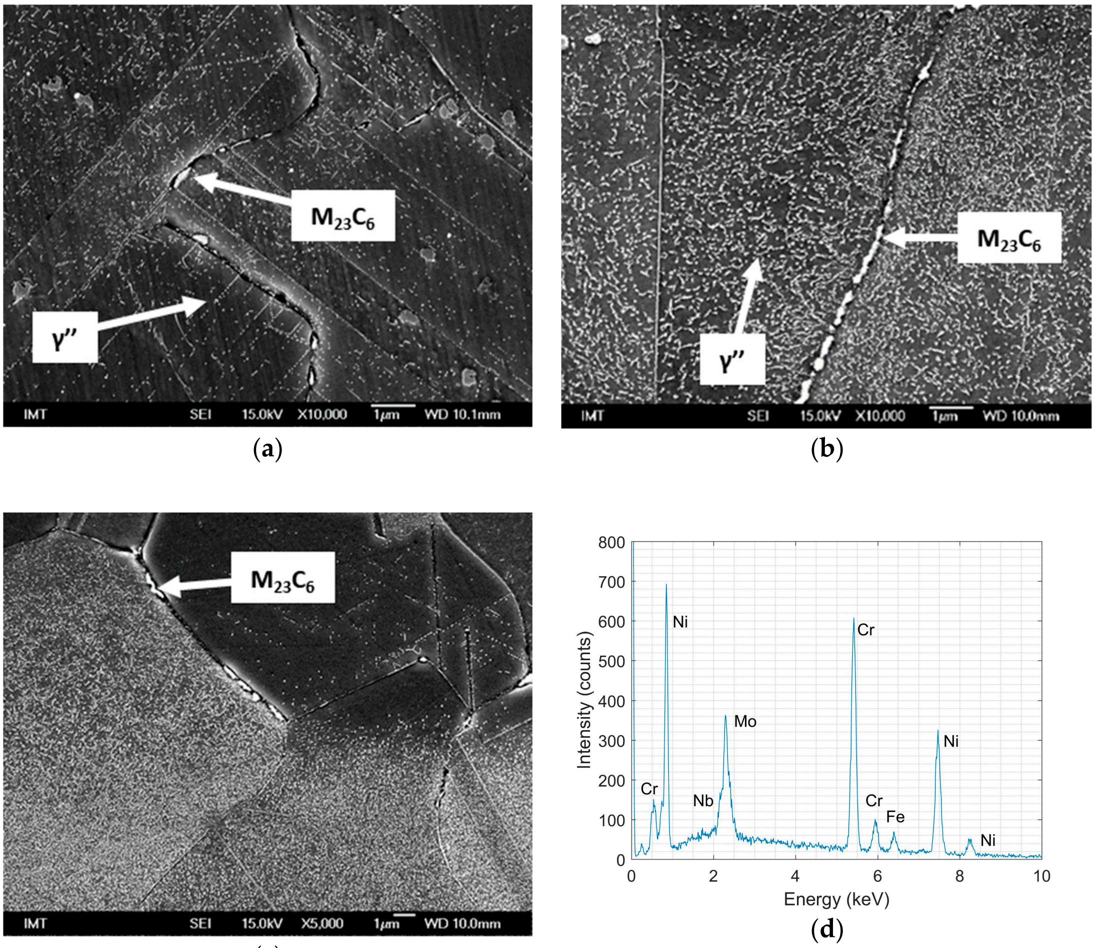

Figure 8. The precipitation of the γ'' in lines in the recrystallized grains of the sample hot rolled at 1050 °C with the deformation level of 23.5% and aged at 750 °C for 1 h (**a**). Secondary $M_{23}C_6$ carbides at the grain boundary in the samples hot rolled at 1150 °C with the deformation level of 5.7% and aged at 750 °C for 5 h (**b**). Precipitation of the secondary $M_{23}C_6$ carbides on the grain boundaries in the sample hot rolled at 1050 °C with the deformation level of 14.4% and aged at 750 °C for 5 h (**c**). The EDS spectrum of the secondary $M_{23}C_6$ carbide in Figure 8c (**d**).

There is no difference in the γ'' precipitate size and density (Figures 10c,d and 11c,d, Table 4) between the deformed and the recrystallized grains within the segregation bands. The centers of the segregation bands have high Nb contents that enable the homogeneous γ'' nucleation (dislocation and twins have no influence) (Figure 9c). In this case, the concentration of Nb (4.7 wt. %) is similar to Inconel 718. At an aging temperature of 750 °C, the start of the γ'' precipitation is below 1h of aging time for Inconel 718 [15,34]. The nucleation of the γ'' phase in Inconel 718 is homogeneous, which may explain our observations in the segregation bands. A high Nb content reduces the critical radius size, thus enabling a large number of fine γ'' precipitates. As soon as the average Nb concentration is lowered (<4.5 wt. %), the critical radius increases and heterogeneous nucleation occurs (Figure 9c). As we move from the center of the segregation band the Nb content is lowered from 4.7 to 2.5 wt. % (Figure 9c). The edge of the segregation band is clearly visible due to the difference in the precipitate size and the distribution in the deformed and recrystallized grains (Figure 8c, Figure 10e,f, and Figure 11e,f, Table 4).

Table 4. The average size and standard deviation of γ'' phase particles in different areas on Figure 11 (sample hot rolled at 1050 °C with the deformation level of 23.5% and aged at 750 °C for 25 h).

Location	Size of γ'' PhaseParticles (nm)
Deformed grain in the segregation band (Figure 11c)	79.7 ± 11.9
Recrystallized grain in the segregation band (Figure 11d)	77.5 ± 11.6
Deformed grain, the inner edge of the segregation band (Figure 11e)	80.4 ± 16.9
Recrystallized grain, the inner edge of the segregation band (Figure 11f)	196.2 ± 63.1
Recrystallized grain in the inner edge of the segregation band (twin) (Figure 11f)	72.7 ± 15.9
Deformed grain in the outer edge of the segregation band (Figure 11a)	66.6 ± 14.3

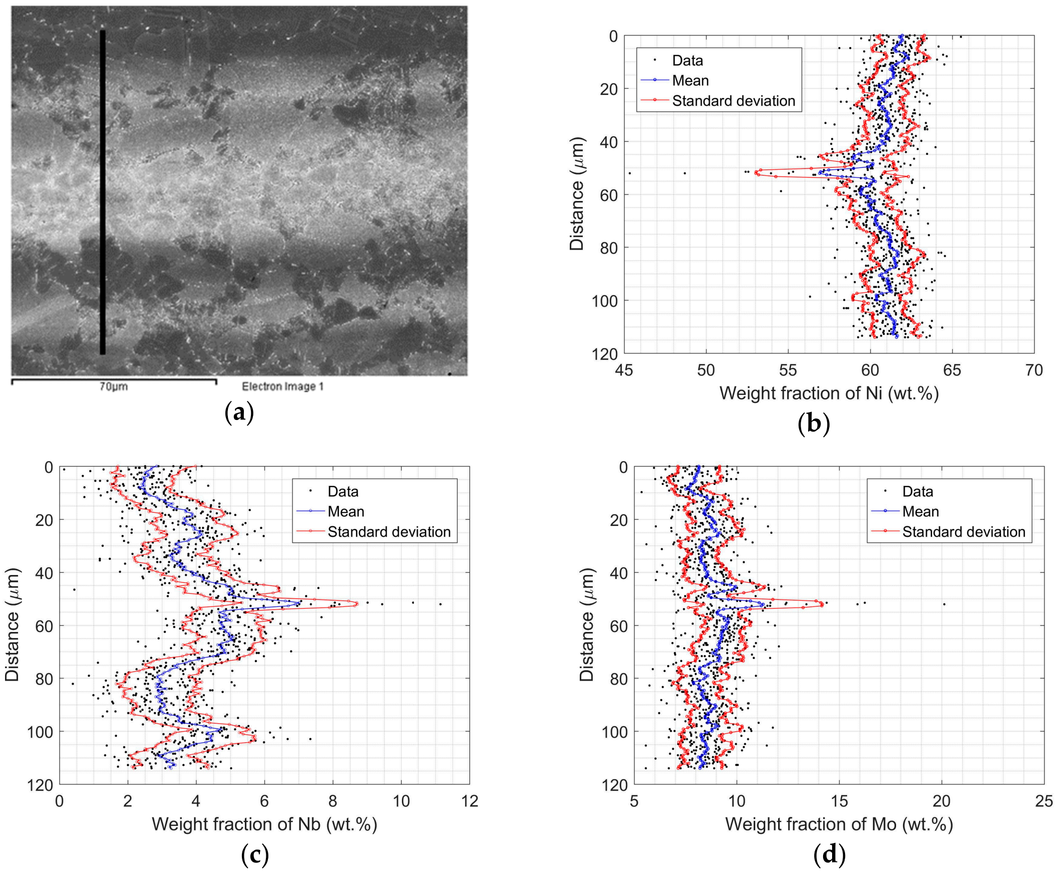

Figure 9. Different segregation bands with different distributions of the γ'' phase precipitate in the sample hot rolled at 1050 °C with the deformation level of 23.5% and aged at 750 °C for 25 h (**a**). Centered moving average (5 wide) and standard deviation of a 5 × 191 (3 µm wide and 127 µm long line) points in a line (**a**), for Ni Kα (**b**), Nb Lα (**c**) and Mo Lα (**d**).

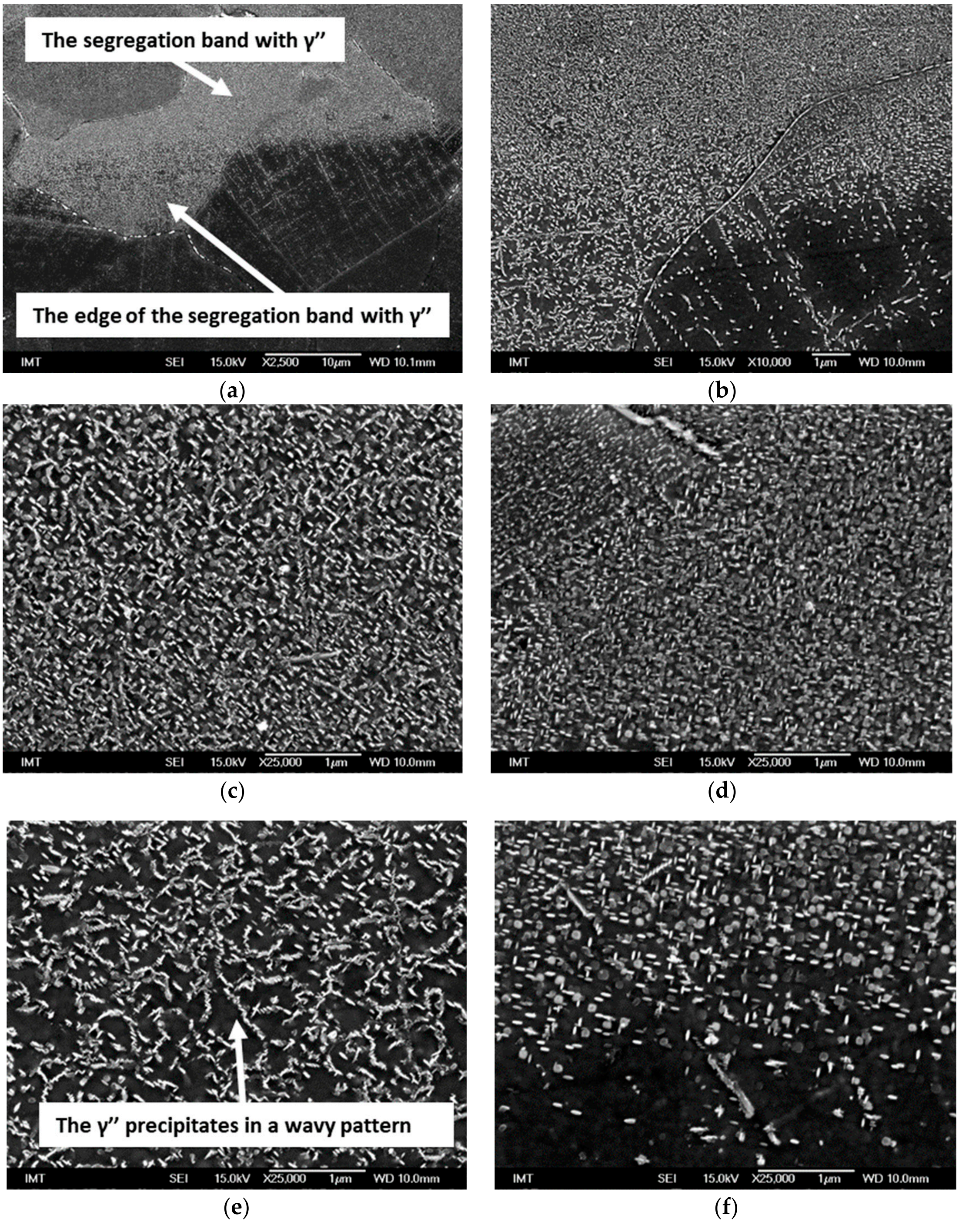

Figure 10. Segregation band of the sample hot rolled at 1150 °C with the deformation level of 14.4% and aged at 750 °C for 5 h (**a**,**b**). The precipitation of the γ'' in the segregation band of deformed grain (**c**) and recrystallized grain (**d**). The wavy pattern of the γ'' precipitates in the deformed grain at the edge of the segregation band (**e**). The γ'' precipitation in recrystallized grain at the inner edge of the segregation band (**f**).

The deformed grains have a smooth transition in terms of the γ'' precipitate number and size (Figure 11c,d, Table 4), as they have high dislocation densities (nucleation sites) (Figures 3b and 12a,b). When the dislocation structure before aging (Figure 3b) and after aging (Figure 10e) is compared the γ'' precipitates form the same wavy-like pattern or lines as dislocations (Figures 5c, 10e and 12b). With the decreasing content of Nb towards the far edge of the segregation band, the size and density of the

γ'' slowly decreases (Table 4). Due to a large number of γ'' precipitates in the deformed grains the coarsening is slow. The large numbers of γ'' precipitates remain even after a longer period of aging (125 h) (Figure 14b).

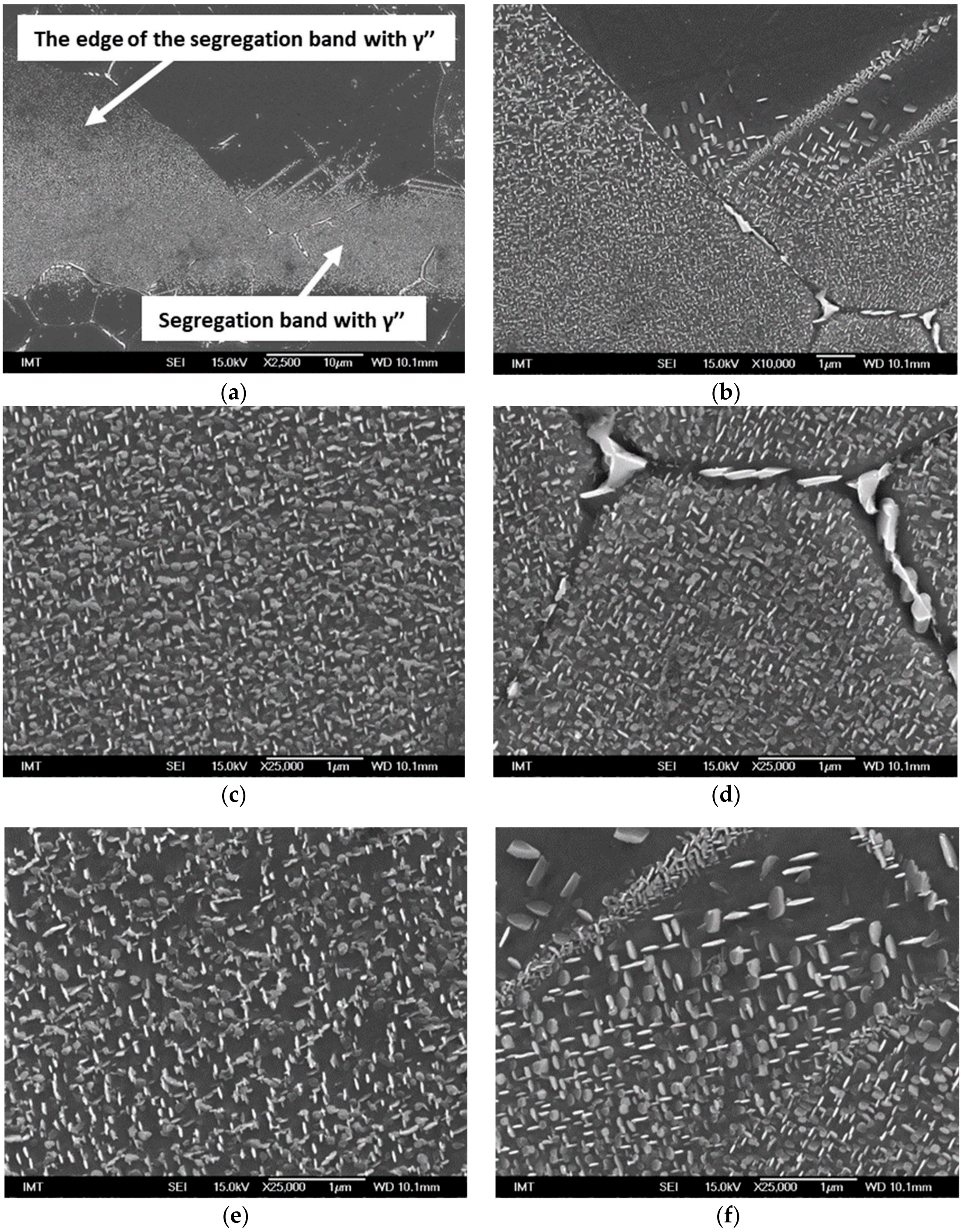

Figure 11. Segregation band of the sample hot rolled at 1050 °C with the deformation level of 23.5% and aged at 750 °C for 25 h (**a**,**b**). The precipitation of the γ'' in the segregation band of the deformed grain (**c**) and the recrystallized grain (**d**). The difference between the precipitation at the edge of the segregation band in the deformed (**e**) and the recrystallized grain (**f**).

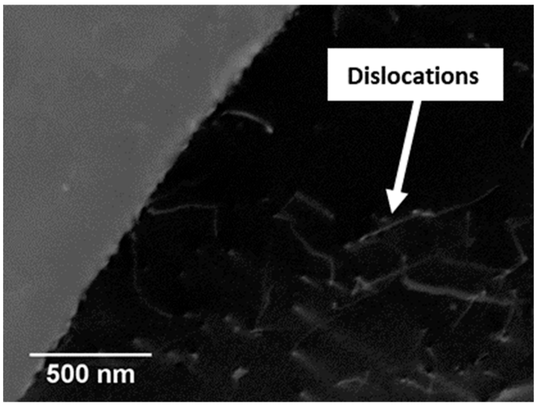

(a)

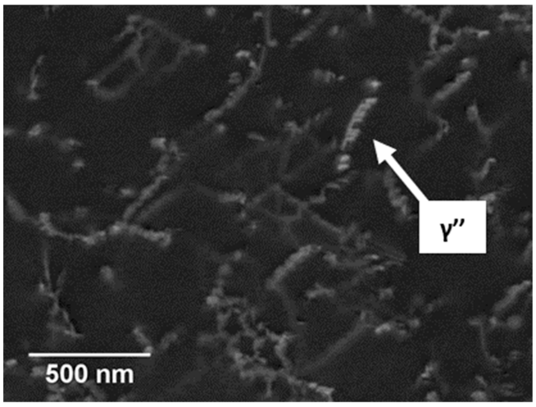

(b)

Figure 12. ECCI image of a sample hot rolled at 1150 °C with the deformation level of 5.7% and aged at 750 °C for 5 h. Dislocations in the deformed grain outside of the segregation band (**a**). The γ'' precipitates and dislocations in the deformed grain at the edge of the segregation band (**b**).

The recrystallized grains do not have a smooth transition in γ'' precipitate size and distribution (Figure 10b,f and Figure 11b,f). When the Nb concentration decreases (Figure 9c), the precipitate size increases and the density decreases for the homogeneously precipitated γ'' (Figure 11f, Table 4). At the same time, the heterogeneous precipitation of γ'' occurs on the twins and dislocations (Figure 10f, Figure 11b,c and Figure 13d,e). The homogeneously precipitated γ'' are prone to more severe coarsening with increasing aging time (5+ h). Due to the lower density of precipitates, the surrounding γ-matrix contains enough Nb to enable larger γ'' precipitate growth (Figure 14a). Thus, the difference in size between heterogeneously and homogeneously precipitated γ'' becomes significant after a longer aging time (25+ h) (Figure 14a). The homogeneously precipitated γ'' disappear with the decreasing content of Nb, and only smaller γ'' precipitates remain on the twins and dislocations (Figure 11b). As we move further from the center of the segregation band (<4 wt. % Nb), even the large numbers of fine γ'' precipitates on twins and dislocations are difficult to see in the recrystallized grains (Figure 11a). Even after a longer aging time at 750 °C (125 h), the precipitation of γ'' did not occur (Figure 14b). During the formation of the nucleus, the γ'' interacts with the dislocation stress field. The stress field of the dislocations can relieve the volume strain energy needed for nucleation [2]. The dislocations have areas strained in compression and tension. So, the nucleus will only form in the area that sufficiently relieves the volume strain energy. This is why the deformed grains contain higher densities of γ'' precipitates. A higher dislocation density in the deformed grains offer more nucleation sites compared to the dislocations and twins in recrystallized grains. Below a 2.7 wt. % Nb concentration, the precipitation of γ'' did not occur in the deformed or recrystallized grains (Figure 9a). The solubility of niobium in Inconel 625 at room temperature is around 2.5 wt. % [5].

The δ phase in the segregation bands of samples aged for 5+ h was observed in the shape of short needles and blocky particles on the grain boundaries (Figure 13a,c–e, Figures 14b and 15a,b) [10]. The needles of the δ phase precipitated in random locations in the grain and on the twins (Figures 13c, 14b and 15a). The EDS measurement showed elevated concentration of Nb typical for δ phase with composition of (Ni_3Nb). The δ phase formed as smooth, continuous lines on the twins (Figure 13c,d). During prolonged aging (25+ h), the δ phase replaced the γ'' precipitates on the twins of the recrystallized grains. However, typically for samples deformed with a higher deformation level, the continuous δ phase lines were not smooth but serrated (Figure 15c,d and Figure 16a). During the hot deformation, the twins formed steps/facets to accommodate the plastic deformation. With the increasing deformation level, the twins transformed into ordinary HAGBs (Figure 4) [30]. So, the δ phase needles precipitated and grew at an angle, as is seen on some HAGBs (Figure 15c,d). There are no precipitates of γ'' around the δ-phase (Figures 15c and 16a). During prolonged aging (25+ h) the metastable γ'' precipitates are consumed due to the growth of the δ phase. The morphology of the δ phase is different outside the segregation bands (Figure 16a,b). Outside of the segregation band, the precipitation of the δ phase did not occur on the twins (Figure 16a,b).

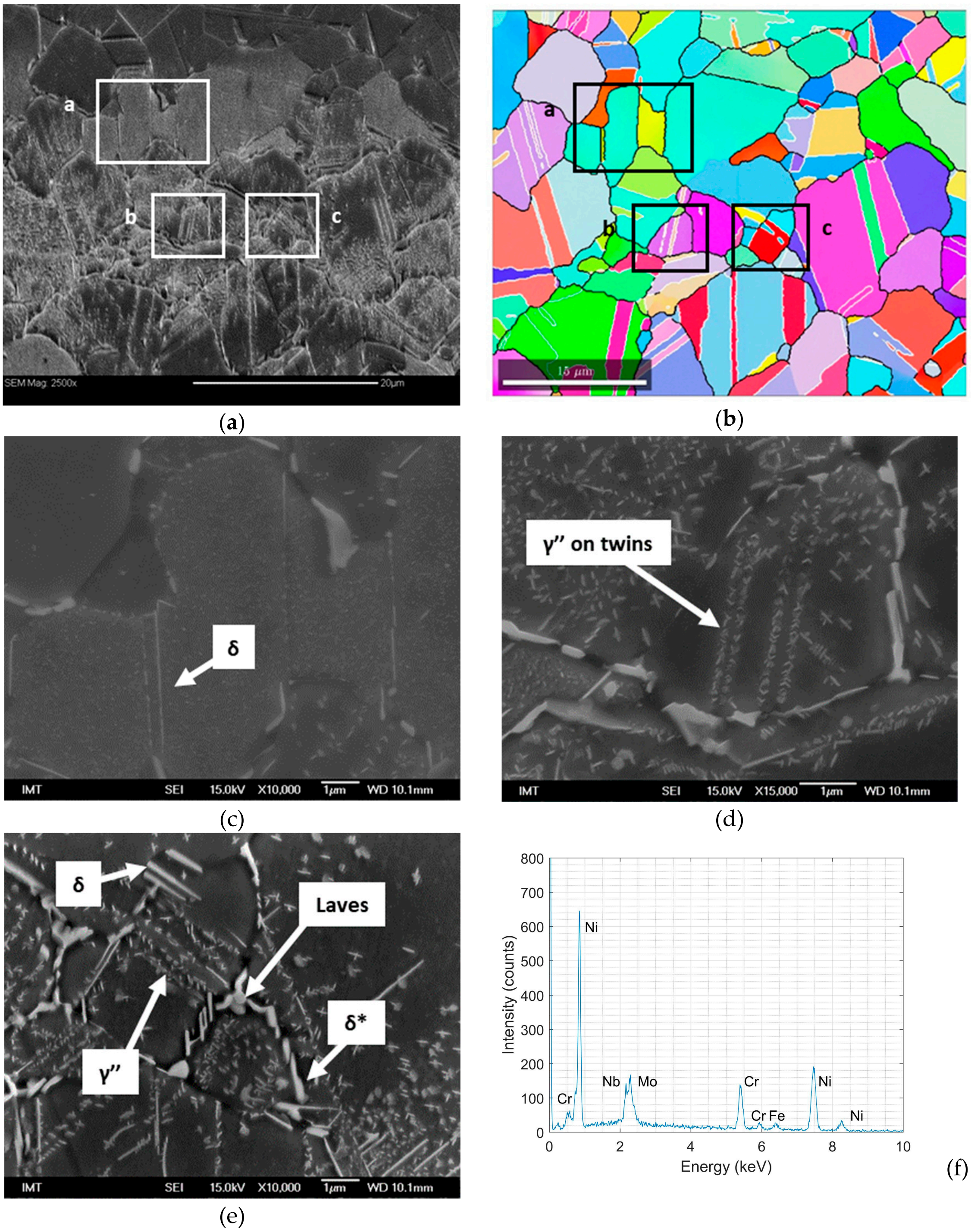

(**a**) (**b**) (c) (d) (e) (f)

Figure 13. The segregation band in the sample hot rolled at 1050 °C with the deformation level of 23.5% and aged at 750 °C for 25 h (**a**). OIM image with IPF-Z coloring of the Figure 13a with black high-angle grain boundaries and white CSL3 boundaries (**b**). Enlarged areas from the Figure 13a of the deformed grain (**c**) in the area a, recrystallized grain with γ″ precipitates on twins in the area b (**d**) and in the area c (**e**). The EDS spectrum (**f**) of δ* phase in Figure 13e.

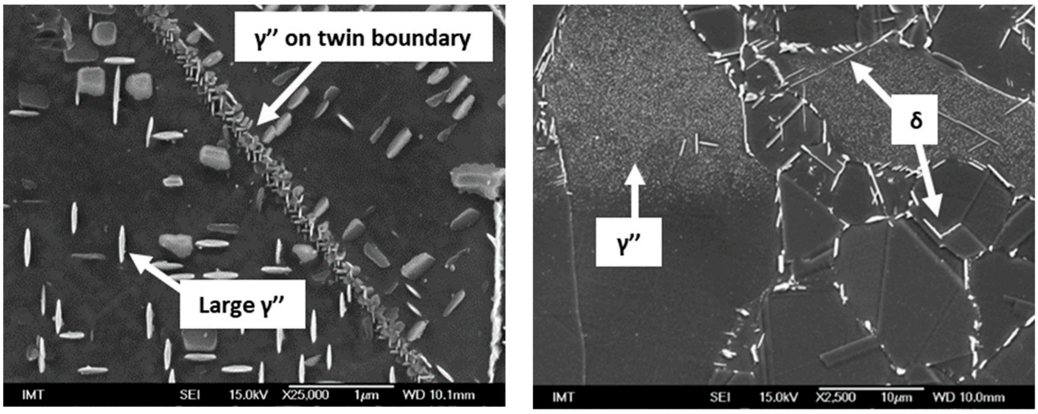

(**a**) (**b**)

Figure 14. Large γ'' precipitates and smaller ones along the twin of the sample hot rolled at 1050 °C with the deformation level of 23.5% and aged at 750 °C for 25 h (**a**). The transition from segregation band in the sample hot rolled at 1150 °C with the deformation level of 25.2% and aged at 750 °C for 125 h (**b**).

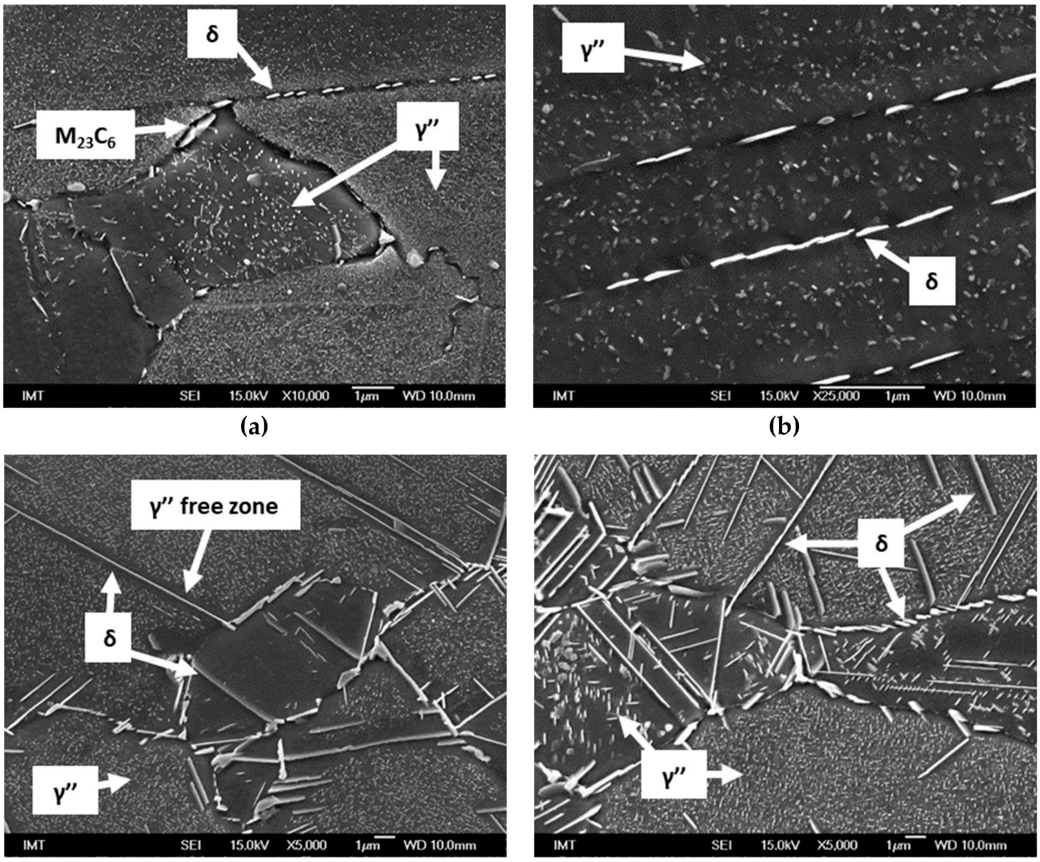

(a) **(b)**

(c) **(d)**

Figure 15. The precipitation of the δ phase in the segregation band of the sample hot rolled at 1050 °C, with the deformation level of 23.5% and aged at 750 °C for 5 h (**a**). The precipitates of the δ-phase needles on twins in the sample hot rolled at 1050 °C with the level of deformation 12.7% and aged at 750 °C for 25 h (**b**). The δ-phase precipitates in the deformed and the recrystallized grain of sample hot rolled at 1050 °C with the deformation level of 12.7% and aged at 750 °C for 125 h (**c**). The precipitation of δ phase in the deformed and the recrystallized grains of the sample hot rolled at 1150 °C with the deformation level of 14.4% and aged at 750 °C for 125 h (**d**).

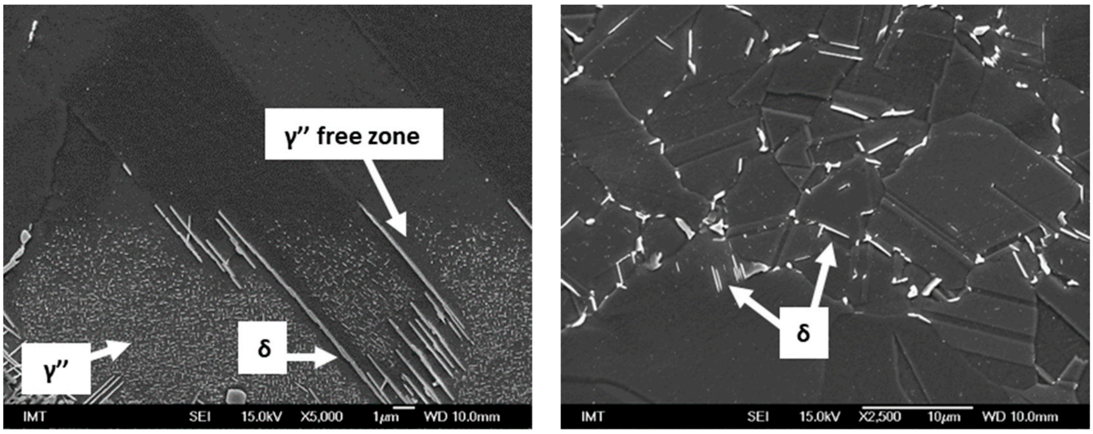

(a) (b)

Figure 16. The precipitation of the δ phase in the transition area of the sample hot rolled at 1050 °C with the deformation level of 12.7% and aged at 750 °C for 25 h (**a**). Different morphology of the δ phase outside the segregation band of the sample hot rolled at 1050 °C with the deformation level of 23.5% and aged at 750 °C for 125 h (**b**).

3.3. Influence of the Segregation Bands, Prior Hot Rolling and Aging on the Room-Temperature Tensile Strength

The yield strength, tensile strength and elongation are plotted in Figure 17. The yield strength and tensile strength increased, while the elongation decreased (Figure 17) with increasing deformation levels due to the strain hardening. Samples hot rolled at 1150 °C have lower yield strength and tensile strength, while the elongation was higher compared to hot rolling at 1050 °C. After aging at 750 °C for 5 h, there was an increase in the yield and tensile strength, and a decrease in the elongation due to the precipitation of γ''. However, after prolonged aging times (25+ h), the yield strength and tensile strength did not change significantly. The increase in the yield and tensile strength after aging for 5 h was the lowest for the samples hot rolled with the highest deformation because of the to a larger volume fraction of recrystallized grains. The yield strength and tensile strength for the hot-rolled plates with the highest deformation level increased after longer aging times (25+ h) due to the precipitation of the δ phase.

Most of the samples had a ductile fracture surface after the tensile test (Figures 18–20). The fracture surface of the tensile-test specimens revealed cracks and particle pull outs. The cracks and pull-outs were seen even in the unaged samples (Figure 18a,b). The cracks originated at segregation bands, due to the primary NbC carbides, the (Nb,Ti)(C,N) carbo nitrides and the TiN nitrides (Figure 20a,b). A cross-section of tensile-test specimens revealed pores in lines. Some pores contained shattered particles (Figure 20b). During the tensile tests, pores formed in the segregation bands, and were connected to each other, thus forming a crack during fracture. After aging, the cracks grew in size and depth, due to the extensive precipitation in the segregation bands (Figure 13d). The hot-rolled sample at 1150 °C, with the deformation level of 5.7% and aged at 750 °C for 5+ h, had an inter-crystalline fracture (Figure 21) due to the precipitation of secondary $M_{23}C_6$ carbides (Figure 8b).

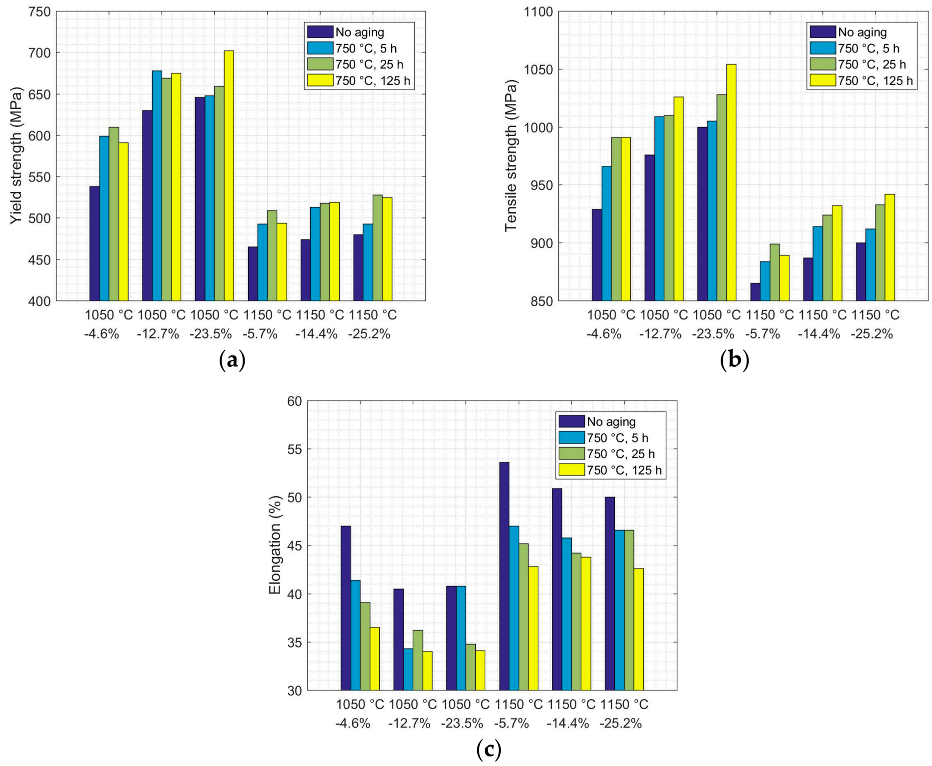

Figure 17. The yield strength (**a**), tensile strength (**b**) and elongation (**c**) for the samples with prior deformation at 1050 and 1150 °C unaged and aged at 750 °C for 5, 25 and 125 h.

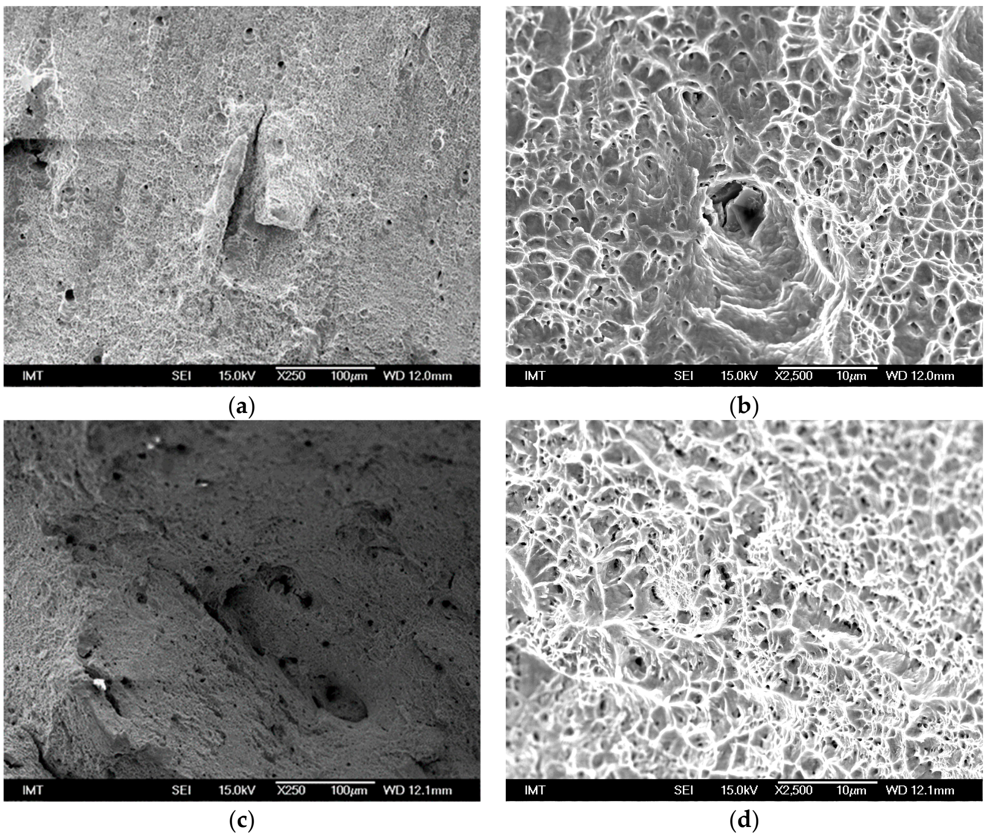

Figure 18. The Fracture surfaces of the samples hot rolled at 1050 °C with the deformation level of 23.5% (unaged) (**a**,**b**) and aged at 750 °C for 5 h (**c**,**d**).

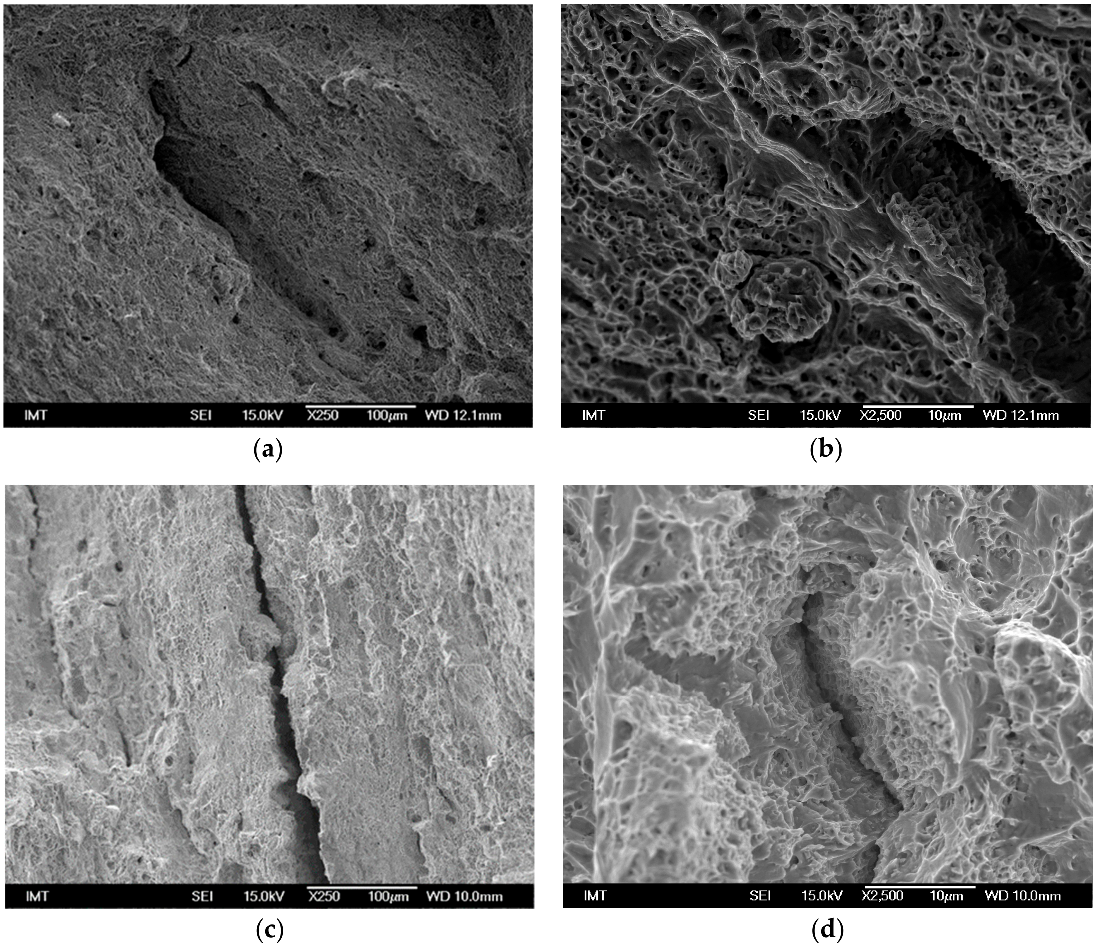

Figure 19. The fracture surface of the samples hot rolled at 1050 °C with the deformation level of 23.5% and aged at 750 °C for 125 h (**a**,**b**). The fracture surface of sample hot rolled at 1050 °C with the deformation level of 12.7% and aged at 750 °C for 125 h (**c**,**d**).

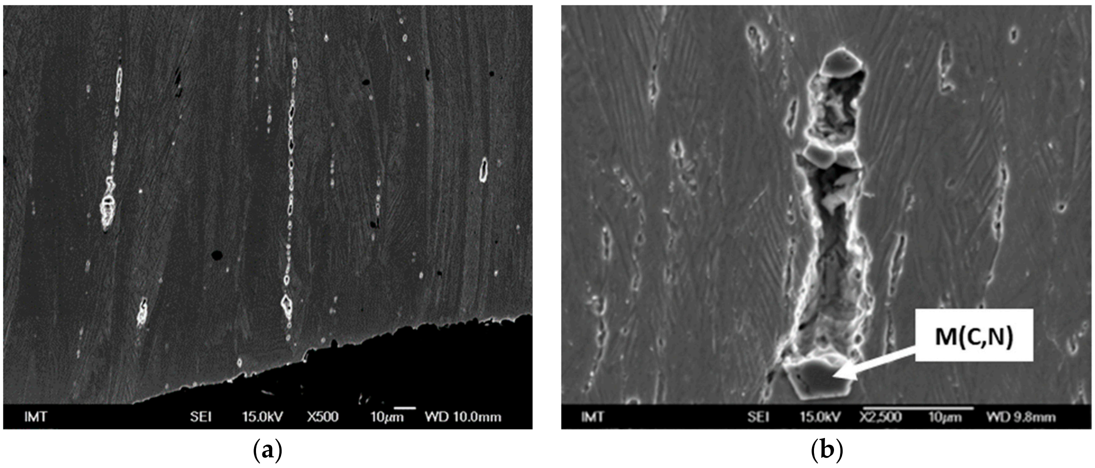

Figure 20. The cross-sections of the sample hot rolled at 1150 °C with the deformation level of 25.2% and aged at 750 °C for 5 h (**a**). Pore with cracked (Nb,Ti)(C,N) carbo nitride in the sample hot rolled at 1050 °C with the deformation level of 23.5% and aged at 750 °C for 5 h (**b**).

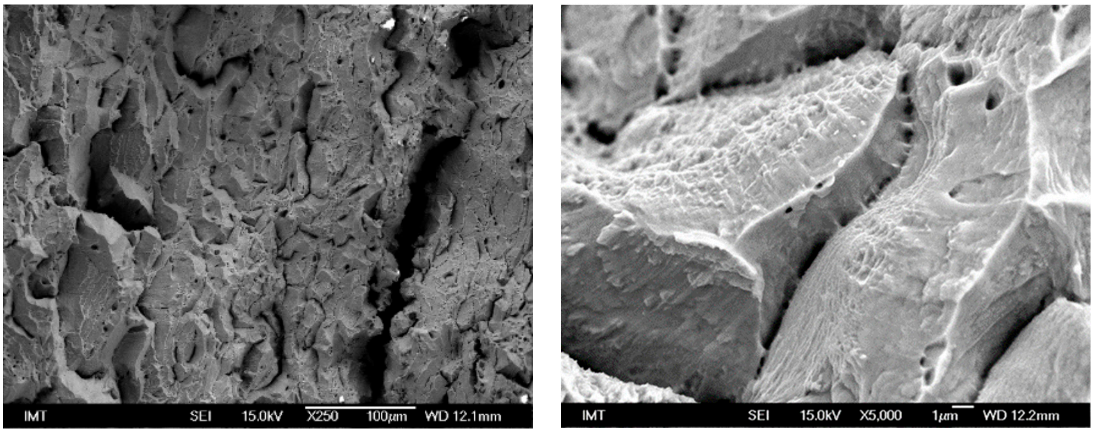

(**a**) (**b**)

Figure 21. The inter crystalline fracture surface of the sample hot rolled at 1150 °C with the deformation level of 5.7% and aged at 750 °C for 5 h (**a**,**b**).

4. Conclusions

The influence of the segregation bands and the prior hot deformation on the precipitation of secondary phases during aging at 750 °C was investigated.

The advantage of the presented method is the simultaneous observation of the γ'' precipitation during aging at 750 °C in deformed grains with a high to low Nb concentration, as well as recrystallized grains with a high to low Nb concentration. This was enabled by the partially recrystallized microstructure and the segregation bands.

A high average concentration of Nb (4.7 wt. %) in the segregation bands promotes the precipitation of the γ'' phase in the deformed and recrystallized grains. The opposite was observed outside the segregation band (<2.7 wt. % Nb) where the precipitation of the γ'' was not observed. The deformed grains promoted the precipitation of large numbers of smaller γ'' precipitates at the edge of the segregation band (2.7 < wt. % Nb < 4.5). A high density of fine γ'' precipitates in the deformed grains increased the tensile strength after 5 h of aging at 750 °C. Due to the lack of nucleation sites in the recrystallized grains, the precipitation of γ'' was severely retarded when the average Nb concentration was reduced (2.7 < wt. % Nb < 4.5). The increase in tensile strength is higher for samples with a lower level of deformation (1050 °C, 4.6% and 12.7% and at 1150 °C 14.4% and 25.2%) and lower for plates with the highest level of deformation (1050 °C, 23.5% and 1150 °C, 25.2%).

Author Contributions: Conceptualization, S.M., J.M. and M.G.; methodology, S.M., F.T., and M.G.; software, S.M., B.Š.B. and F.V.; validation, S.M.; formal analysis, S.M.; investigation, S.M.; resources, M.G. and F.T.; data curation, S.M., B.Š.B. and F.V.; writing—original draft preparation, S.M.; writing—review and editing, J.M., B.Š.B., F.V., J.B., and M.G.; visualization, S.M.; supervision, J.M., J.B. and M.G.; funding acquisition, M.G.

Funding: The authors acknowledge the financial support from the Slovenian Research Agency (research core funding No. P2-0132 and young researcher founding 38186).

Conflicts of Interest: The authors declare no conflict of interest.

References

1. Sundararaman, M.; Mukhopadhyay, P. Heterogeneous Precipitation of the γ'' Phase in Inconel 625. *Mater. Sci. Forum* **1985**, *3*, 273–280. [CrossRef]
2. Aaronson, H.I.; Enomoto, M.; Lee, J.K. *Mechanisms of Diffusional Phase Transformations in Metals and Alloys*; CRC Press: Boca Raton, FL, USA, 2010; ISBN 9781420063004.
3. Prikhodko, S.V.; Ardell, A.J. Coarsening of γ' in Ni-Al alloys aged under uniaxial compression: III. Characterization of the morphology. *Acta Mater.* **2003**, *51*, 5021–5036. [CrossRef]

4. Matysiak, H.; Zagorska, M.; Balkowiec, A.; Adamczyk-Cieslak, B.; Cygan, R.; Cwajna, J.; Nawrocki, J.; Kurzydłowski, K.J. The Microstructure Degradation of the IN 713C Nickel-Based Superalloy After the Stress Rupture Tests. *J. Mater. Eng. Perform.* **2014**, *23*, 3305–3313. [CrossRef]
5. Eiselstein, H.L.; Tillack, D.J. The Invention and Definition of Alloy 625. In *Superalloys 718, 625 and Various Derivatives (1991)*; TMS: Warrendale, PA, USA, 1991; pp. 1–14.
6. Cortial, F.; Corrieu, J.M.; Vernot-Loier, C. Influence of heat treatments on microstructure, mechanical properties, and corrosion resistance of weld alloy 625. *Metall. Mater. Trans. A* **1995**, *26*, 1273–1286. [CrossRef]
7. Shankar, V.; Bhanu Sankara Rao, K.; Mannan, S. Microstructure and mechanical properties of Inconel 625 superalloy. *J. Nucl. Mater.* **2001**, *288*, 222–232. [CrossRef]
8. Sundararaman, M.; Kumar, L.; Prasad, G.E.; Mukhopadhyay, P.; Banerjee, S. Precipitation of an intermetallic phase with Pt2Mo-type structure in alloy 625. *Metall. Mater. Trans. A* **1999**, *30*, 41–52. [CrossRef]
9. Evans, N.D.; Maziasz, P.J.; Shingledecker, J.P.; Yamamoto, Y. Microstructure evolution of alloy 625 foil and sheet during creep at 750 °C. *Mater. Sci. Eng. A* **2008**, *498*, 412–420. [CrossRef]
10. Suave, L.M.; Cormier, J.; Villechaise, P.; Soula, A.; Hervier, Z.; Bertheau, D.; Laigo, J. Microstructural Evolutions During Thermal Aging of Alloy 625: Impact of Temperature and Forming Process. *Metall. Mat. Trans. A* **2014**, *45*, 2963–2982. [CrossRef]
11. Moore, I.J.; Burke, M.G.; Palmiere, E.J. Modelling the nucleation, growth and coarsening kinetics of γ''(D022) precipitates in the Ni-base Alloy 625. *Acta Mater.* **2016**, *119*, 157–166. [CrossRef]
12. Tian, Y.; Ouyang, B.; Gontcharov, A.; Gauvin, R.; Lowden, P.; Brochu, M. Microstructure evolution of Inconel 625 with 0.4 wt% boron modification during gas tungsten arc deposition. *J. Alloys Compd.* **2017**, *694*, 429–438. [CrossRef]
13. Cieslak, M.J.; Headley, T.J.; Romig, A.D.; Kollie, T. A melting and solidification study of alloy 625. *Metall. Trans. A* **1988**, *19*, 2319–2331. [CrossRef]
14. Hin Ac, C.; Brechet, Y.; Maugis Cd, P.; Soisson, F. Heterogeneous precipitation on dislocations: Effect of the elastic field on precipitate morphology. *Philos. Mag.* **2008**, *88*, 1555–1567. [CrossRef]
15. Qin, H.; Bi, Z.; Yu, H.; Feng, G.; Du, J.; Zhang, J. Influence of stress on γ'' precipitation behavior in Inconel 718 during aging. *J. Alloys Compd.* **2018**, *740*, 997–1006. [CrossRef]
16. Zhang, H.; Li, C.; Liu, Y.; Guo, Q.; Huang, Y.; Li, H.; Yu, J. Effect of hot deformation on γ'' and δ phase precipitation of Inconel 718 alloy during deformation&isothermal treatment. *J. Alloys Compd.* **2017**, *716*, 65–72. [CrossRef]
17. Azarbarmas, M.; Aghaie-Khafri, M.; Cabrera, J.M.; Calvo, J. Dynamic recrystallization mechanisms and twining evolution during hot deformation of Inconel 718. *Mater. Sci. Eng. A* **2016**, *678*, 137–152. [CrossRef]
18. Humphreys, F.L. *Recrystallization and Related Annealing Phenomena*; Elsevier: Amsterdam, The Netherlands, 2004; ISBN 0080982697.
19. Tian, B.; Zickler, G.A.; Lind, C.; Paris, O. Local microstructure and its influence on precipitation behavior in hot deformed Nimonic 80a. *Acta Mater.* **2003**, *51*, 4149–4160. [CrossRef]
20. Li, D.; Guo, Q.; Guo, S.; Peng, H.; Wu, Z. The microstructure evolution and nucleation mechanisms of dynamic recrystallization in hot-deformed Inconel 625 superalloy. *Mater. Des.* **2011**, *32*, 696–705. [CrossRef]
21. Tehovnik, F.; Burja, J.; Podgornik, B.; Godec, M.; Vode, F. Microstructural evolution of Inconel 625 during hot rolling. *Mater. Tehnol.* **2015**, *49*, 801–806. [CrossRef]
22. Guo, Q.; Li, D.; Peng, H.; Guo, S.; Hu, J.; Du, P. Nucleation mechanisms of dynamic recrystallization in Inconel 625 superalloy deformed with different strain rates. *Rare Met.* **2012**, *31*, 215–220. [CrossRef]
23. Krakow, R.; Bennett, R.J.; Johnstone, D.N.; Vukmanovic, Z.; Solano-Alvarez, W.; Lainé, S.J.; Einsle, J.F.; Midgley, P.A.; Rae, C.M.F.; Hielscher, R. On three-dimensional misorientation spaces. *Proc. R. Soc. A Math. Phys. Eng. Sci.* **2017**, *473*, 20170274. [CrossRef] [PubMed]
24. Barr, C.M.; Leff, A.C.; Demott, R.W.; Doherty, R.D.; Taheri, M.L. Unraveling the origin of twin related domains and grain boundary evolution during grain boundary engineering. *Acta Mater.* **2018**, *144*, 281–291. [CrossRef]
25. Prithiv, T.S.; Bhuyan, P.; Pradhan, S.K.; Subramanya Sarma, V.; Mandal, S. A critical evaluation on efficacy of recrystallization vs. strain induced boundary migration in achieving grain boundary engineered microstructure in a Ni-base superalloy. *Acta Mater.* **2018**, *146*, 187–201. [CrossRef]
26. Sharma, N.K.; Shekhar, S. Cut-off deviation for CSL boundaries in recrystallized face-centered cubic materials. *Philos. Mag.* **2017**, *97*, 2004–2017. [CrossRef]

27. McCarley, J.; Tin, S. Understanding the effects of recrystallization and strain induced boundary migration on ∑3 twin boundary formation in Ni-base superalloys during iterative sub-solvus annealing. *Mater. Sci. Eng. A* **2019**, *740–741*, 427–438. [CrossRef]
28. Gutierrez-Urrutia, I.; Zaefferer, S.; Raabe, D. Coupling of Electron Channeling with EBSD: Toward the Quantitative Characterization of Deformation Structures in the SEM. *Jom* **2013**, *65*, 1229–1236. [CrossRef]
29. Zhang, J.-L.; Zaefferer, S.; Raabe, D. A study on the geometry of dislocation patterns in the surrounding of nanoindents in a TWIP steel using electron channeling contrast imaging and discrete dislocation dynamics simulations. *Mater. Sci. Eng. A* **2015**, *636*, 231–242. [CrossRef]
30. Jiang, H.; Dong, J.; Zhang, M.; Yao, Z. Evolution of twins and substructures during low strain rate hot deformation and contribution to dynamic recrystallization in alloy 617B. *Mater. Sci. Eng. A* **2016**, *649*, 369–381. [CrossRef]
31. Zupanič, F.; Bončina, T.; Križman, A.; Tichelaar, F. Structure of continuously cast Ni-based superalloy Inconel 713C. *J. Alloys Compd.* **2001**, *329*, 290–297. [CrossRef]
32. Mu, Y.; Wang, C.; Zhou, W.; Zhou, L. Effect of Nb on δ Phase Precipitation and the Tensile Properties in Cast Alloy IN625. *Metals* **2018**, *8*, 86. [CrossRef]
33. Hu, Y.L.; Lin, X.; Yu, X.B.; Xu, J.J.; Lei, M.; Huang, W.D. Effect of Ti addition on cracking and microhardness of Inconel 625 during the laser solid forming processing. *J. Alloys Compd.* **2017**, *711*, 267–277. [CrossRef]
34. Lass, E.A.; Stoudt, M.R.; Katz, M.B.; Williams, M.E. Precipitation and dissolution of δ and γ'' during heat treatment of a laser powder-bed fusion produced Ni-based superalloy. *Scr. Mater.* **2018**, *154*, 83–86. [CrossRef]